2. Chemistry

2-1. Dynamical Change of the Jahn-Teller Effect of Ni in a Cathode Material of Li Secondary Battery as Revealed by in situ XAFS

A lithium ion rechargeable battery is composed of a cathode of lithium transition metal oxide and an anode of graphite, as illustrated in Fig. 1 [1]. This battery is charged by Li deintercalation from the cathode, and is discharged by Li deintercalation from the graphite. Industrially, spinel manganese oxide $LiMn_2O_4$ is a promising cathode material substituted for $LiCoO_2$, which is currently used in commercially available batteries. A battery with a $LiMn_2O_4$ cathode is operated at around 4 V vs. Li/Li^+. $LiMn_2O_4$ has advantages over $LiCoO_2$ because of the low cost of Mn and its favorable environmental characteristics. However, it has disadvantages concerning its cyclic reversibility, showing a significant capacity loss with repeated charge-discharge cycles. Because of this problem, possible improvements in the cyclic reversibility have been widely investigated. Substitution of Mn^{3+} by transition metals is one of the solutions. Recently, Kawai et al. discovered that $Li(Mn,Ni)_2O_4$ cathode material exhibits a 4.7 V working voltage after the 4.3 V plateau [2]. However, the mechanism responsible for this high potential during the charge-discharge process has remained unsolved. An XAFS analysis of the cathode materials will provide useful information for understanding the electrochemical behavior of the cathode materials. The present study was made to reveal the variations in the chemical states and the local structure of the Mn and Ni ions in a $Li_{1-x}Mn_{1.7}Ni_{0.3}O_4$ cathode material as a function of the Li content by an in situ XAFS analysis.

We have developed an in-situ XAFS cell incorporating a thin-film cathode, a liquid electrolyte, and a lithium foil anode [3]. The Mn and Ni K-XAFS spectra were measured by the conventional transmission mode at various stages of the charge process. The measurements were carried out at BL-7C and 12C. The sample weights of the cathodes were adjusted in order to maintain the optimum thickness for the transmission measurements. The cell was charged to a desired voltage at a constant current, then kept in a resting condition for ca. 40 min. The ordinate scale of the XANES spectra was normalized at 500 eV above the absorption edge.

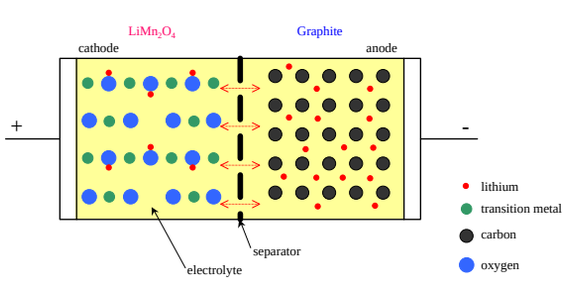

Figure 1.
A schematic illustration of the principle of the Li ion secondary battery.

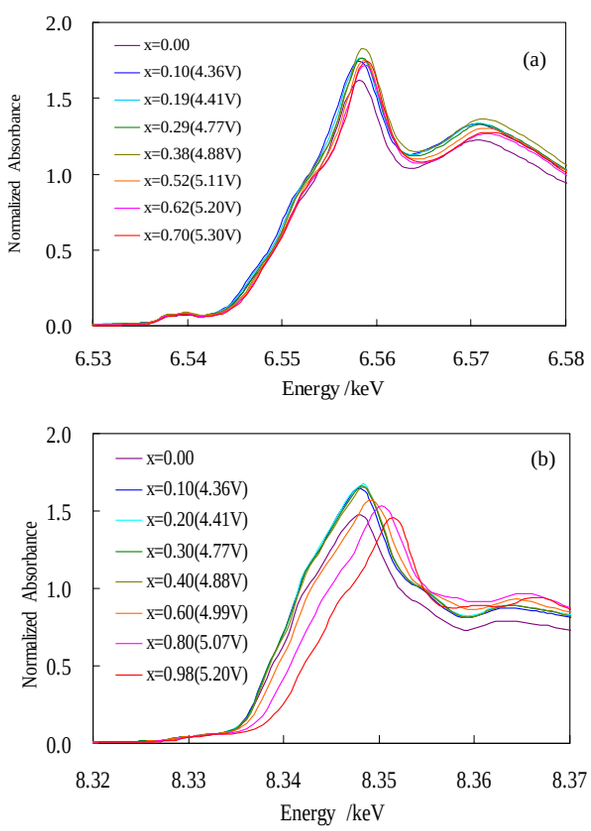

Figure 2.
(a) Mn K-edge XANES spectra and (b) Ni K-edge XANES spectra of $Li_{1-x}Mn_{1.7}Ni_{0.3}O_4$ as a function of the Li content (1−x).

The Mn K-XANES spectra of $Li_{1-x}Mn_{1.7}Ni_{0.3}O_4$ as a function of x are shown in Fig. 2(a). The Li concentrations (1-x) were estimated from the known cathode masses and the total charge. The voltage values given in Fig. 2 are the open-circuit voltages of the cell. As can be seen from Fig. 2(a), the Mn K-edge absorption energy shifts to the higher energy side with an increase in x, indicating that Mn^{3+} is oxidized to Mn^{4+} with the Li deintercalation. In contrast, the Ni K-edge spectra (Fig. 2(b)) begin to shift at x = 0.4, and the chemical shift is extremely large (the total shift is as large as 4.2 eV). The existence of Ni^{2+} in the initial cathode material, $Li_{1-x}Mn_{1.7}Ni_{0.3}O_4$, at x = 0 has been confirmed by a comparison of the Ni K-XANES spectrum with those of reference materials. This large chemical shift is due to the oxidation of Ni^{2+} to Ni^{4+}. Consequently, a XANES analysis has revealed that the voltage plateau of the cell at 4.3 V arises from the Mn^{3+}- Mn^{4+} redox pair, while the oxidation of Ni^{2+} to Ni^{4+} is responsible for the high-energy plateau at 4.7eV.

Fourier transforms (FT) of the k^3-weighted Ni K-edge EXAFS oscillations of the samples are shown as a function of x in Fig. 3. The first peak at around 1.5 Å in FT corresponds to the Ni-O interaction in the first coordination sphere, and the second peak at around 2.5 Å is due to the Ni-(Mn, Ni) interaction in the second coordination sphere. Although the intensities of the Ni-(Mn, Ni) peaks increase with the Li deintercalation, the Ni-O peak height shows a peculiar variation. The height of the Ni-O peak begins to decrease when x exceeds 0.4, and reaches to a minimum at x = 0.6. The peak then increases significantly with a further deintercalation of Li. An extraordinarily small Ni-O peak was also observed in the FT of $LiNiO_2$ [4]. It was reported that such a small peak was caused by a Jahn-Teller distortion of the Ni^{3+}-O_6 octahedron [4]. Similarly, the small Ni-O peak observed for the phase at x = 0.6 can be ascribed to the distorted Ni-O octahedron due to the Jahn-Teller effect of Ni^{3+}. Consequently, it was found that Ni^{2+} is first oxidized to the low-spin Ni^{3+}, which is the d^7 Jahn-Teller ion; then, when x exceeds 0.6, Ni^{3+} starts to oxidize to Ni^{4+}. Since the charge-discharge cycles accompanies a large volume change in the NiO_6 octahedra of the cathode due to the Jahn-Teller effect, this material will not be suitable for the cathode of the rechargeable battery. Thus, dynamical changes in the Ni oxidation state and its coordination polyhedron with the Li deintercalation of the cathode material has been clearly elucidated experimentally for the first time [5]. The present study has also demonstrated that the XAFS technique is suitable for the in situ characterization of various electrochemical reactions.

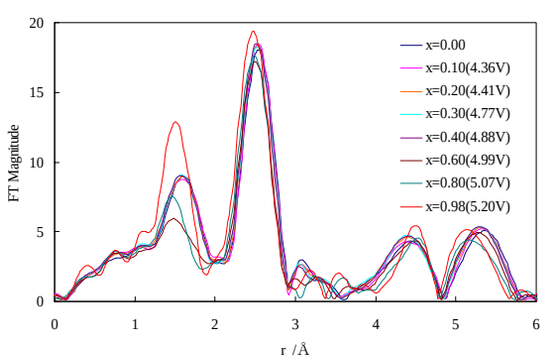

Figure 3.
Fourier transforms of Ni K-edge EXAFS spectra of $Li_{1-x}Mn_{1.7}Ni_{0.3}O_4$ as a function of the Li content (1–x).

Y. Terada[1], K. Yasaka[1], I. Nakai[1] and M. Yoshio[2]
([1]Science Univ. of Tokyo and [2]Saga Univ.)

References

[1] K. Brandt, Solid State Ionics 69 (1994) 173.
[2] H. Kawai, N. Nagata, H. Tsukamoto and A. R. West, J. Power Sources 81-82 (1999) 67.
[3] I. Nakai, Y. Shiraishi and F. Nishikawa, Spectrochim. Acta B54 (1999) 143.
[4] I. Nakai, K. Takahashi, Y. Shiraishi, T. Nakagome and F. Nishikawa, J. Solid State Chem. 140 (1998) 145.
[5] Y. Terada, K. Yasaka, F. Nishikawa, T. Konishi, M. Yoshio and I. Nakai, J. Solid State Chem. 156 (2001) 286.

2-2. XAFS Studies on Actinide Chemistry [1]

Actinide chemistry contributes to the peaceful use of atomic energy techniques from the following two points: 1) the development of recycling methods of fissile materials from spent fuel, and safety-disposal methods of the radioactive wastes, and 2) the discovery of effective usage in other fields. Additionally, 5*f* electronic states in actinide compounds are attracting considerable interest due to their intermediate nature between rare-earth 4*f* and transition-metal 3*d* electrons from the viewpoint of fundamental research. The experiments that need a macro volume of actinides, i.e. electronic-structure and structural studies, however, are severely hampered by the radioactivity and toxicity of these materials. Therefore, the widespread use of such techniques as well as synchrotron-radiation facilities have stimulated extreme progress to actinide science. The BL-27 of PF, the only beamline where radioactive materials including actinides can be handled in Japan, has been constructed in a collaboration between KEK and JAERI. The following studies were performed at BL-27. We are preparing further applications of XAFS to the minor actinides, i.e., Np, Am, and Cm by using a special chamber at BL-27B.

The local structures of uranium (VI)-amide complexes in solution were determined by EXAFS spectroscopy at BL-27B for the development of nuclear reprocessing. An understanding of the coordination polyhedron is required for molecular modeling of the separation agent of these metals, since the coordination of the ligand causes various kinds of separation phenomena. Figure 1 shows the radial structural function of the uranium-amide (N,N-dihexyl-2-ethylhxane amide: DH2EHA) complex in ethanol. Amide, which consists of biological materials, i.e., C, H, O, and N, and is incinerable, will not produce further radioactive waste, compared to phosphorous compounds, such as tributylphosphate (TBP). The peak at 1.5 Å in Fig. 4 is the typical structure in

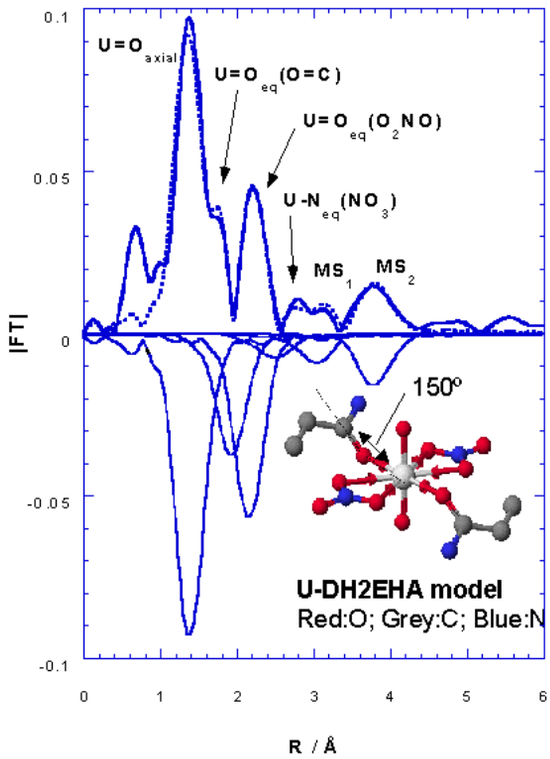

Figure 4.
Fourier transform (without phase corrections) of the k^3-weighted EXAFS spectra of the U (VI)-DH2EHA complex in ethanol solution. The solid line is the experimental data, and the dashed line is the theoretical fit. Shown negative FT amplitudes are single shell contribution to fit. The illustration in the figure shows the cluster of U (VI)-DH2EHA complex.

uranyl oxygen on the axial, and the peaks at about 2.0 Å arise from the oxygen of carbonyl groups and nitrate ions on the equatorial plane. The bond angle of U-O(carbonyl group)-C(carbonyl group) was estimated to be about 150° based on the structural parameters in this study, suggesting that the chemical bond property between uranium and the amide might be ionic. These results have suggested that amide compounds have sufficient abilities as substitute of TBP.

As mentioned above, the electronic-structure of actinide is expected to have very unique properties. From the viewpoint of basic actinide sci-

ence, we measured the U-L_{III} XANES spectra of uranium metallofullerenes at BL-27B. The valence state of the encapsulated uranium has been estimated based on the chromatographic behavior of the metallofullerenes. The candidate structure of U@C_{82}, estimated from La@C_{82} [2], is shown in the illustration of Fig. 5. Until now, direct information of the valence state of uranium has not yet been obtained. Figure 5 shows the U-L_{III} XANES spectra of uranium metallofullerences (U@C_{82} and U_2@C_{80}) and several compounds. The edge energies of uranium were determined by two ways: 1) as inflection point of the edge estimated by the 2nd derivative and 2) as the energy of arctangent in least-squares fits of the XANES region using an arctangent plus Gaussian functions. In Fig. 5, the energies by method 1) were shown by solid lines. These energies were assigned to the $2p_{3/2} \rightarrow 6d$ transition. The chemical shifts of UCl_3 and $UO_2(NO_3)_2$-$2H_2O$ in this study were about −5eV and about 1.6 eV from UO_2, respectively. These differences are essentially the difference in the Coulomb interaction between the $2p_{3/2}$ core hole and the 5f electronic states of these compounds, and demonstrate the screening power of an additional 5f electron. The shift values of the uranium metallofullerences (U@C_{82} and U_2@C_{80}) were approximately equal to UCl_3, suggesting that the uranium encapsulated in the fullerences were +3. On the basis of a general understanding of the uranium oxidation state, uranium is +6 ~ +4 in atmospheric condition, especially the +3 state is stable only in a reducing condition. Accordingly, it has been clarified that the carbon cage condition was a very reducing condition.

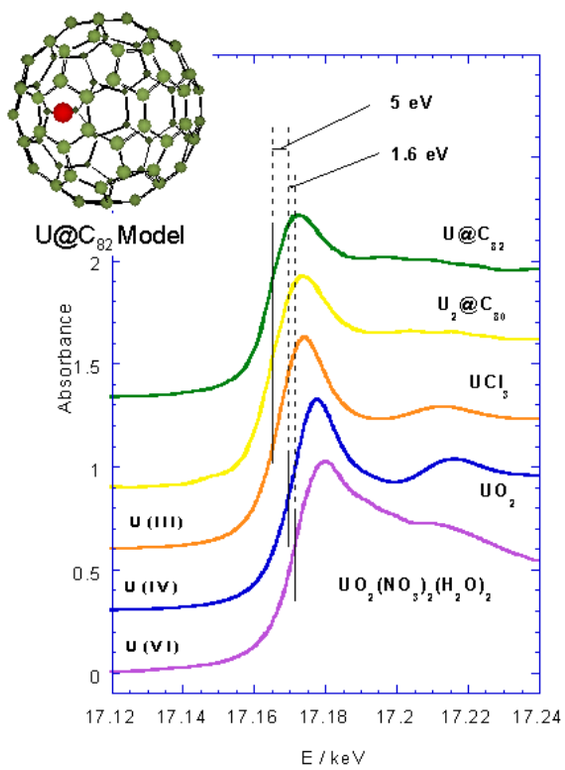

Figure 5.
U-L_{III} XANES spectra of uranium metallofullerenes and uranium compounds. The solid and dashed lines are the inflection points of U L_{III} edge for each compound. The energy difference of these compounds means those from UO_2. The illustration in the figure shows the candidate structure of U@C_{82}, estimated from La@C_{82} [1].

T. Yaita, Y. Okamoto, and K. Akiyama (JAERI)

References

[1] T. Yaita et al., submitted to OECD/NEA report , Inorg. Chem. and JACS (2001).
[2] H. Suematsu et al., Mat. Res. Soc. Symp. Proc., 349 (1994) 213.